A Final Report

# INVESTIGATION OF THE QUANTUM EFFICIENCY OF OPTICAL HETERODYNE DETECTORS

Submitted to:

National Aeronautics and Space Administration
Langley Research Center
Hampton, VA 23665

Attention: Mr. Daniel J. Jobson
FED, M/S 473

Submitted by:

T. E. Batchman
Associate Professor

Report No. UVA/528212/EE85/101

November 1984



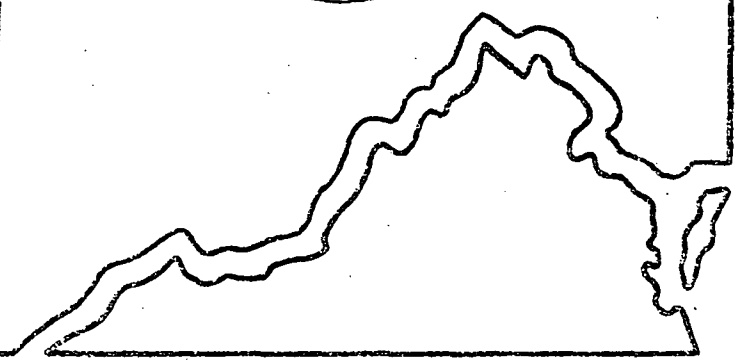

UNIVERSITY OF VIRGINIA

COMPUTER ENGINEERING AND CONTROL LABORATORY
DEPARTMENT OF ELECTRICAL ENGINEERING
SCHOOL OF ENGINEERING AND APPLIED SCIENCES
UNIVERSITY OF VIRGINIA

FINAL REPORT

GRANT NO. NASA - NAG-1-262

# INVESTIGATION OF THE QUANTUM EFFICIENCY OF OPTICAL HETERODYNE DETECTORS

Submitted By

T. E. Batchman
Associate Professor

Report No. UVA/528212/EE85/101
September 1984

TABLE OF CONTENTS

ABSTRACT

This research program investigated the frequency response and quantum efficiency of optical photodetectors for heterodyne receivers. The measurements utilized two spectral lines from the output of two lasers as input to the photodetectors. These lines were easily measurable in power and frequency and hence served as known inputs. By measuring the output current of the photodetector the quantum efficiency was determined as a function of frequency separation between the two input signals. An investigation of the theoretical basis and accuracy of this type of measurement relative to similar measurements utilizing risetime was undertaken.

A theoretical study of the heterodyne process in photodetectors based on semiconductor physics was included so that higher bandwidth detectors may be designed. All measurements were made on commercially available detectors and manufacturers specifications for normal photodetector operation are compared to the measured heterodyne characteristics.

## Technical Summary

Laser heterodyne systems have recently come to the forefront of technology for gas concentration measurements, remote sensing applications and communication systems. Applications have included planatary and atmospheric studies, exhaust analysis, possible rocket plume detection and Doppler Lidars [1]. Usually the system employed for these measurements uses the near infrared wavelength region, however, a visible wavelength system is possible and for some applications is desired. These applications include oceanographic temperature and salinity measurements, chlorophyll and oil detection and possible applications in connection with blue-green laser communication for submarines.

One of the chief requirements for a heterodyne system is a wide-bandwidth photomixer. This is one of the difficulties in a visible heterodyne system, because the normal photodetector has a bandwidth of less then 1 GHz. For temperature and salinity measurements, a bandwidth of 8 GHz is desired. This study evaluated photodetectors to be used as mixing elements (photomixer) for such a system.

The desired feature for this application is a detector with high quantum efficiency at high frequencies and low noise to yield a high signal-to-noise ratio. The low noise can be achieved partially by having a low dark current; a quantity which is easy to measure. The quantum efficiency is considerably more difficult to measure and was subject to this study.

Previously, the frequency response (and hence quantum

efficiency) of a photodetector was found by measuring the shot noise spectrum of the device. This type of measurement is very misleading and at most is useful for only a maximum response spectrum [2]. Recently the frequency dependent quantum efficiency has been measured in heterodyne applications by measuring signal-to-noise ratios [3-5].

In this study the quantum efficiency as a function of frequency was measured using two single mode laser sources which could be tuned to give a frequency separation varying between 100 MHz ad 10 GHz. The input optical powers to the photodetector and the output current were then measured and the quantum efficiency was calculated. These measurements cover the output frequency range from dc to 10 GHz and are taken between pairs of wavelengths in the 537-580 μm region.

A detailed theoretical analysis was undertaken and is presented in a Ph.D disseration, ref. 12. From this analysis more efficient photodiodes can be designed. Data supplied by the photodetector manufactures was used to calculate the expected frequency response of the detectors and this response was compared to the measured response. The calculated responses only agreed with the measurements when mounting and package capacitances were estimated as measured.

The results of this study are summarized in the attached paper submitted for publication. Additional measurements are found in reference 12 along with a more detailed discussion of the measurement technique.

# INTRODUCTION

Fiber optic heterodyne systems and heterodyne remote sensing applications have recently received increasing interest [1-3]. These applications usually require photodetectors with frequency responses in the GHz range [3].

In applications such as space based LIDAR systems, exact knowledge of the photodetector frequency response is required. While there has been much theoretical work done on heterodyne detection, this theory has not been confirmed with true device heterodyne frequency response measurements. This paper will confirm the theory and present measurements on several devices.

The photodetector, when used as the mixing element in a heterodyne system, is usually a semiconductor p-n or p-i-n junction device. In the optical spectrum, these devices act as particle detectors or quantum-mechanical square-law detectors. An output current at the difference frequency is produced when two electro-magnetic waves with proper alignment are incident on the detector [4-9].

The semiconductor detectors are usually operated in a reverse bias mode, creating a large electric field in the depletion region of the diode. When the incident radiation, having an energy per photon greater than the bandgap of the semiconductor is absorbed, electron-hole pairs are created. The electron-hole pairs created in the depletion region are swept away by the large electric field creating a drift current. Any minority carriers created outside this region that can diffuse to the depletion region will also be swept across by the electric

field creating a diffusion current. Both of these response processes, drift and diffusion, have a characteristic response time and thus a characteristic frequency response.

There are two major methods of illuminating the detectors. In front illumination, which is the method usually used, the radiation propagates parallel to the electric field (Fig. 1a). This method creates non-uniform generation since along the direction of current flow the number of carriers will vary due to the exponential absorption of the radiation. Side-illumination produces uniform generation since the absorption is orthogonal to the electric field, and hence the direction of current flow, Fig. 1b.

## FREQUENCY RESPONSE OF THE DRIFT AND DIFFUSION PROCESSES

Lucousky, et al, have presented the response for the drift process with both uniform and non-uniform generation [10]. For uniform generation with incident flux $\Phi$, the generation rate is

$$g = \alpha\Phi \exp(-\alpha y)[1 + A \exp(j\omega t)] \qquad (1)$$

where $\alpha$ is the material absorption coefficient and $\omega$ is the difference frequency. The induced real current density is given by

$$J(y,t) = g\alpha\Phi\exp(-\alpha y)\, w\, [1 + A \cos(\omega t + \phi)|F|] \qquad (2)$$

where w is the width of the depletion region and F is the frequency response function given by equation 1a in the appendix. The phase angle, $\phi$, is the arctan $[I_m(F)/Re(F)]$.

The generation rate for non-uniform generation is given by

$$g = \Phi\alpha \exp(-\alpha x)[1 + A \exp(j\omega t)] \tag{3}$$

and the frequency response function is considerably more complex as equation 2a shows (see appendix). This illumination method yields the faster response time of the two methods. Figure 2 shows the non-uniform frequency response for values representative of silicon at 0.51 μm wavelength radiation. As shown, with thin depletion regions ($\leq$ μm), bandwidths in excess of 10 GHz can be expected from the drift process.

Unless steps are taken to eliminate it, however, there will be a current produced due to the diffusion process. This process, previously discussed by Sawyer et al. [11], is much slower, and therefore, yields much lower bandwidths. For uniform generation the induced diffusion current is given by [11, 12]

$$J_{dc} = \frac{-q\alpha\Phi\exp(-\alpha y)L}{s - \frac{D_n}{L}} \left[s\left(1-\exp\left(\frac{x_p}{L}\right)\right) = \frac{D_n}{L} \frac{s \cosh \frac{x_p}{L} + \frac{D_n}{L} \sinh \frac{x_p}{L}}{s \sinh \frac{x_p}{L} + \frac{D_n}{L} \cosh \frac{x_p}{L}}\right] \tag{4}$$

$$J_{ac} = -q\alpha\Phi\exp(-\alpha y)\, A \exp(j\omega t)\, L_c \left[1 - \frac{s\left(1-\exp\left(-\frac{x_p}{L}\right)\right) + \frac{D_n}{L_c} \exp\left(-\frac{x_p}{L_c}\right)}{(s)\sinh\left(\frac{x_p}{L_c}\right) + \frac{D_n}{L_c} \cosh\left(\frac{x_p}{L_c}\right)}\right] \tag{5}$$

where the total current is given by $J_{dc} + J_{ac}$, L is the diffusion length, $x_p$ is the p region thickness, $D_n$ is the electron velocity carrier diffusion coefficient and $L_c$ is the complex diffusion length given by

$$L_c = \left(\frac{D_n}{1/\tau_n + j\omega}\right)^{1/2} \tag{6}$$

The frequency response function is given by $J_{ac}/J_{dc}$ with the modulation factor, A, equal to unity. Non-uniform generation

yields an induced current of



$$J_{dc} = -q\Phi G(L) \tag{7}$$

$$J_{ac} = -Aq\Phi\exp(j\omega t)G(L_c) \tag{8}$$

where

$$G(L) = \frac{1}{1-\frac{1}{\alpha^2 L^2}}\left[\left(\frac{s}{\alpha D_n}+1\right)-\exp(-\alpha x_p)\cdot\frac{\left(\frac{s}{\alpha D_n}+1\right)\cosh\left(\frac{x_p}{L}\right)+\left(\frac{1}{\alpha L}+\frac{sL}{D_n}\right)\sinh\left(\frac{x_p}{L}\right)}{\cosh\left(\frac{x_p}{L}\right)+\left(\frac{sL}{D_n}\right)\sinh\left(\frac{x_p}{L}\right)}\right] \tag{9}$$

Figure 3 shows the frequency response for non-uniform generation using material values representative of low-doped silicon at 0.51 um. Bandwidths on the order of 1 GHz can be obtained using thin regions (<1 um). This process obviously has a much lower response than the drift process.

## RC EFFECTS

Regardless of the current producing process, the drift process or diffusion process, the RC time constant of the diode will also affect the frequency response of the diode. The 3 dB frequency due to this effect is given by

$$f_{RC} = w/[2\pi(R_S + R_L)\varepsilon A_d] \tag{10}$$

where $R_S$ is the diode series resistance, $R_L$ is the diode load resistance and the junction capacitance is given by $\varepsilon A_d/w$ where $A_d$ is the device area and $\varepsilon$ is the material permitivity.

Having a knowledge of these frequency limiting processes, general device design guidelines can be formulated [12] and

frequency response predictions can be made from known diode parameters.

## EXPERIMENTAL MEASUREMENT PROCEDURE

The heterodyne efficiencies have been measured for several devices using the apparatus of Fig. 4. Here, two tunable single frequency Argon-ion lasers are used to generate the optical signals to the photodetector. The photodetector, which is being characterized, is connected to a microwave power meter so the output difference frequency power can be measured. A second mixer diode is used in the system to detect the difference frequency for display on a RF spectrum analyzer to provide frequency and stability information. An optical spectrum analyzer is also used to check spectral purity and stability of the two optical signals.

A focusing lens is used to focus the radiation on the detector. The focal length of this lens is determined by the size of the detector; the focused spot size is chosen to match the detector size. For a circular detector of radius p intercepting 98% of the incident radiation the focal length is given by,

$$f = \frac{\pi p a}{\lambda \sqrt{2}} \qquad (11)$$

where a is the incoming gaussian beam intensity radius (1/e points) and $\tau$ is the wavelength of operation.

A coherent Innova 90 and a Lexel model 75 were used as the sources. The beam radius on these lasers were different (0.75 mm for the coherent and 0.45 mm for the Lexel) and thus the maximum mixing efficiency obtainable is 78% [12, 13, 8] so if absolute

measurements are desired this factor must be considered.

The device efficiency is measured at a particular frequency by measuring the power ($P_C$,$P_L$) from each laser incident on the focusing lens and the output of the detector as measured on the microwave power meter, $p_\mu$. The efficiency is then given by

$$\eta = \left(\frac{p_\mu}{p_C p_L}\right)^{1/2} \frac{h\nu}{q} \frac{1}{(1-R)} \frac{1}{(2z)^{1/2}} \qquad (12)$$

where h is Plack's constant, $\nu$ is the optical frequency, z is the load impedance. R is taken as the combined reflection coefficients of the lens, detector window and device surface so that internal quantum efficiency is obtained.

## DEVICE MEASUREMENTS

Several commercial devices have been characterized by the measurement system described. Two of these devices were high bandwidth or ultra-fast response detectors. The other detectors characterized were available in our laboratory and were characterized only for comparison with those presented here [12]. Results for the two fast response detector are summarized in this section.

The Ford Aerospace L4502 specifications are given in Table 1. A computer simulation of the fabrication process was provided by the manufacturer. This simulation generates an impurity profile for the device which can then be used to find the depletion region width and the p-layer thickness. These were found to be 1.5 um and 2.2 um, respectively, which indicates that 89% of the radiation is absorbed in the p-layer and 9% is absorbed in the depletion region. The remaining 2% is absorbed

in the n region. This device will be diffusion process limited since most of the radiation is absorbed in the p-layer. The junction capacitance was also predicted to be approximately 1 pf which is lower than the specifications, however considering package effects and fringing the comparison is reasonable.

The average measured dc efficiency of the device at 0.514 um is 40%. Much higher efficiencies were measured in localized areas using a short focal length (2.5 cm) lens. These measurements are shown in Table 2. This variation in efficiency indicates the field distribution will effect the measurements if the frequency response also varies across the detector. [8, 14] A window transmission factor of 0.9, a theoretical air-silicon interface transmission factor of 0.94 or 0.91 for the 2.5 cm and 20.0 cm focal length lens, respectively are assumed. Since these values were not measured the quantum efficiencies have some uncertainty associated with them. It can only be stated that the average efficiency of the entire device, including window and the surface reflection at 0.514 um, is 22%.

Ac measurements on the device yield Figs. 5 and 6. These measurements use the same transmission factors as discussed for the dc measurements. These figures also show the measured dc efficiencies for the respective measurement runs. The difference between the dc efficiencies and the low frequency ac efficiencies is due to the mixing efficiency. In all cases the difference is almost exactly the 78% that was predicted by considering the field distributions.

The measured data plotted in Fig. 5 shows that variations in

the frequency response do occur across the surface of the detector. These measurements were taken with a 2.5 cm focal length lens, thus yielding spot sizes of 8 um and 13 um for the Coherent and Lexel lasers respectively. These measurements, therefore, are not indicative of the entire detector, but of various spots on the detector. The variations do not appear to be severe, but the measured efficiencies will vary somewhat depending on the optical field distributions used to make the measurements.

Figure 6 shows the efficiencies measured using a 20.0 cm focal length lens. This response is representative of the entire device since this lens produces spot sizes of 60 um and 100 um for the Coherent and Lexel lasers respectively. This figure clearly indicates three major areas of operation. At low frequencies diffusion current dominates, producing the majority of the current at frequencies less than a few hundred MHz. At frequencies near 1 GHz the diffusion current has rolled off and the drift current dominates. Above this frequency RC rolloff occurs and the response decreases at approximately 10 dB/decade.

Using the measured average dc efficiency, the depletion region and p-region widths found above, a theoretical prediction of the response can be made. This prediction is made by weighting the response of each region by the absorption efficiency of that region to obtain a total predicted response. So that direct comparison to the measured data can be made, the total response is then weighted by an RC rolloff factor with a 3 dB frequency of 2 GHz. The 2 GHZ rolloff frequency is equivalent to a 50 ohm load, a series resistance of 5 ohms, and a junction

capacitance of 1.5 pf. These numbers are reasonable for this device and the data seems to indicate that rolloff occurs at this frequency. The p-region response is obtained by using a surface recombination velocity such that a total dc efficiency of 40% is obtained. The predicted response is shown as the solid curve in Fig. 7. This response was obtained using a diffusion coefficient of 10 $cm^2/sec.$ for the P-region, corresponding to an impurity level of $2 \times 10^{18}$ $cm^{-3}$. A n-region diffusion coefficient of 2.5 $cm^2/sec$ was used which also corresponds to an impurity level of $2 \times 10^{18}$ $cm^{-3}$.

The predicted response compares very well with the measured data at frequencies below 2 GHz. Above 2 GHz the response rolls off at 17 dB/decade indicating that more than a single RC pole exists. This implies that the package and the contacts from the package to the diode are affecting the response. The equivalent circuit for the diode, package and bias Tee is shown in Fig. 8. It has been shown [12] that if the package capacitance is negligable the microwave detector current, $I_L$, supplied to the 50 ohm microwave power meter load, $R_L$, is given by

$$\frac{I_L}{I_{photo}} = \frac{1}{j\omega C_j(j\omega L_p + R_p + R_L + R_s) + 1} \qquad (13)$$

The diode is mounted on the center post of a BNC connector with the p-region connected to the outside conductor of the connector through a 25 um diameter, 0.238 cm (3/32") long wire. Assuming a copper wire, the high frequency impedance of this wire is [15]

$$Z = 3.32 \times 10^{3} \sqrt{f} \ (1 + j) \text{ ohms} \tag{14}$$

Using this to determine $R_p$ and $\omega L_p$ the package effects can be included and the resultant response is calculated using (13) and is shown in Fig. 9. Comparing these curves to Fig. 7, the measured response iss between that predicted by a 2 GHz RC rolloff and the calculated inductor rolloff. Since the package capacitance has been neglected, and a theoretical value for the impedance of the wire has been used, it is not suurprising that the calculated rolloff was greater than measured.

The response without the 2 GHz RC rolloff or the package effects is shown in Fig. 9 as the short circuit response. Since the device is also available in a better microwave package, this short circuit response is representative of what performance could be expected from the photodiode in a better package operating into a low impedance load. Figure 10 shows the frequency response of the individual processes. As can easily be seen the bandwidth is limited by the response of the p-layer. The bandwidth of the n-layer is not high either, but this region only absorbs 3% of the incident radiation. This device is thus limited in bandwidth severely by the thick p-layer.

The specifications for the Opto-Electronics PD-015-03 detector are listed in Table 3. The impulse response measured by the manufacturer is shown in Fig. 11 and as this and the specifications show the risetime of the device is 355 psec.

As the dc measurements in Table 4 indicate, a vast range of dc efficiencies were obtained. It is likely that this is partly due to saturation effects. The short focal length lens, yielding smaller spot sizes and thus higher power densities consistantly yielded lower efficiencies. The last five measurements (three measurements with the Lexel laser and two with the Coherent) in the table show a steadily increasing efficiency for each laser when lower power was used. It is thus probable that saturation of the detector was occuring, however, if this did occur it did not affect the frequency response as will be seen later. It is hard to accurately determine the quantum efficiency without being able to measure the transmission factor of the window and the reflection coefficient of the silicon. Here the measured transmission factor of the focusing lens (0.91 or 0.94), the estimate of the transmission factor of the detector window (0.9), and the transmission factor of the air-silicon interface (0.6) [13] were used to calculate the efficiency. The average efficiency of the entire device including window and reflection due to the photodetector surface is 51%.

Several ac sets of measurements were taken on this device, the results of which are shown in Figs. 12 and 13. These figures show efficiencies obtained using two different focusing lenses. The data shown in figure 12 was taken with the 2.5 cm focal length lens, which allows the detector to be probed for variations in quantum efficiency across the surface of the device. As this figure shows, the device seems to have very consistant characteristics since the curves do not vary from one measurement set to the next.

Figure 13 shows the measurements obtained with a focusing lens having a 15.24 cm focal length. This yielded spot diameters of 45.6 um and 76.2 um for the Coherent and Lexel laser respectively. Since the detector is 85 x 115 um in size, this lens provides a reasonable measurement of the average response of the detector. While these measurements do not compare absolutely, the relative frequency response is identical. It is felt that the difference in absolute levels is due to a combination of the alignment of the system and device saturation and not to variances in the quantum efficiency of the device. The saturation effect has been discussed above and as can be seen in Table 4 variations occur even in the dc measurements.

All of the measurements compare very well in terms of the frequency response as shown in Fig. 14. This figure shows all of the measurement runs; each of which has been normalized by its low frequency value. Since the power density incident on the detector varied due to the focusing lens, saturation effects would have affected the frequency response and would appear here as variations between measurement runs. This does not occur and therefore, saturation effects on the frequency response are negligable.

The 3 dB bandwidth in Fig. 14 is 1300 MHz. This seems to disagree greatly with the 35 picosecond specification. This specification, however, is a risetime specification and is not equivalent to the steady state response time. The transient response shown in Fig. 11 is similar to the impulse response of an RLC circuit given by [16]

$$V_o = \frac{2k}{(1-k^2)^{1/2}} \exp(-2\pi kt/T)\sin[2\pi(1-k^2)^{1/2}t/T] \qquad (15)$$

where, T is the free period and the parameter k is a function of the resistance, capacitance, and inductance in the circuit. This parameter can be found by comparing the magnitude of the first peak to that of the first valley. For this case, k is 0.5. The free period here extends from the beginning of the response to a point slightly beyond the beginning of the second peak (Fig. 15). This period of approximately 200 psec is the characteristic response time which dictates steady state behavior. The 3 dB bandwidth in terms of the free period is given by [16]

$$f_{3dB} = 0.35/T \qquad (16)$$

Thus, the steady state bandwidth that could be expected from this detector is 1.75 GHz. This is in good agreement with the 1300 MHz shown in Fig. 12 and even better agreement with the 1600 MHz obtained from Fig. 13 considering only the measurements taken with the large spot sizes.

## CONCLUSION

The measurements on the two available detectors indicate the theory used to predict the detector response is accurate. The measurements also indicate the difference in rise time measurements as compared to steady state response measurements. This steady state response time can be as much as five to ten times slower than the transient response time.

These theories can be used to develop high bandwidth design

guidelines. For fast detector response, the diffusion current should be eliminated. This can be done by using ultra-thin p-layers or side illumination possibly with the use of an optical fiber. The depletion region thickness should then be tailored for maximum dc efficiency, maximum RC bandwidth and minimum drift process response time.

ACKNOWLEDGEMENTS

The authors would like to thank Ford Aerospace Corp. and Opto-Electronics, Ltd. for supplying the detectors used in these measurements.

## APPENDIX

The frequency response functions presented here were developed in reference 12 and follow the same general development as in reference 10. In our case is the difference frequency between the two incident optical signals and $v_h$ is the hole saturation velocity. The ratio of the electron to hole mobility is b and it has been assumed that a high reverse bias has been applied so that saturation velocities occur across the depletion region. The uniform generation frequency response function is

$$F = \left[\left(\frac{v_h}{w\omega}\right)^2 \left(1-\cos\frac{w\omega}{v_h}\right) + \left(\frac{bv_h}{w\omega}\right)^2 \left(1-\cos\frac{w\omega}{bv_h}\right)\right] \tag{1a}$$

$$-j\left[\left(\frac{v_h}{w\omega}\right)\left(1-\operatorname{sinc}\frac{w\omega}{v_h}\right) + \left(\frac{bv_h}{w\omega}\right)\left(1-\operatorname{sinc}\frac{w\omega}{bv_h}\right)\right]$$

The non-uniform generation frequency response function is

$$F = \frac{\alpha w}{(\alpha w)^2+\left(\frac{\omega w}{v_h}\right)^2}\left[1 - \frac{\exp(-\alpha w)}{1-\exp(-\alpha w)}\operatorname{sinc}\frac{\omega w}{2v_h}\left(\alpha w\cos\frac{\omega w}{2v_h} - \right.\right.$$

$$\left.\left. - \frac{\omega w}{v_h}\sin\frac{\omega w}{2v_h}\right)\right] + \left(\frac{\alpha w}{(\alpha w)^2+\left(\frac{\omega w}{bv_h}\right)^2}\right)\left[-1 + \frac{1}{1-\exp(-\alpha w)}\operatorname{sinc}\frac{\omega w}{2bv_h}\right.$$

$$\left.\left(\alpha w\cos\frac{\omega w}{2bv_h} + \frac{\omega w}{bv_h}\sin\frac{\omega w}{2bv_h}\right)\right] + j\,\frac{\alpha w}{(\alpha w)^2 + \left(\frac{\omega w}{v_h}\right)^2} \tag{2a}$$

$$\left[\frac{\omega}{\alpha v_h} - \frac{\exp(-\alpha w)\operatorname{sinc}\frac{\omega w}{2v_h}}{1-\exp(-\alpha\omega)}\left(\frac{\omega w}{v_h}\cos\frac{\omega w}{2v_h} - \frac{\omega w}{v_h}\sin\frac{\omega w}{2v_h}\right)\right]$$

$$+ j\,\frac{\alpha w}{(\alpha w)^2 + \left(\frac{\omega w}{bv_h}\right)^2}\left[\frac{\omega}{\alpha b v_h} - \frac{\operatorname{sinc}\frac{\omega w}{2bv_h}}{(1-\exp(-\alpha w))}\left(\frac{\omega w}{bv_h}\cos\frac{\omega w}{2bv_h} - \right.\right.$$

$$\left.\left. - \alpha w\sin\frac{\omega w}{2bv_h}\right)\right.$$

REFERENCES


1. Y. Yamamoto, "Receiver Performance Evalation of Various Digital Optical Modulation-Demodulation Systems in the 0.5-10um Wavelength Region," IEEE Journal of Quantum Electronics, Vol. QE-16, No. 11 (November 1980), pp. 1251-1259.

2. T. Okoshi, "Heterodyne and Coherent Optical Fiber Communications: Recent Progress," IEEE Trans. on Microwave Theory and Techniques, Vol. MTT-30, No. 8 (August 1982), pp. 1138-1148.

3. NASA, "Laser/Heterodyne Measurement of Temperature and Salinity," Technical Support Package LAR-12766, 1981.

4. M. C. Teich, "The Physics of Heterodyne Detection in the Far Infrared: Transition from Electric-Field to Photon Absorption Dectection in a Simple System," Proceedings of Heterodyne Systems and Technology, NASA Publication 2138, March 25-27, 1980, pp. 1-10.

5. R. J. Glauber, in Quantum Optics and Electronics, C. de Witt, A. Blandin, and C. Cohen-Tannoudji, Eds., New York: Gordan and Breach Science Publishers, Inc., 1965, pp. 75-76.

6. C. Teich, "Field Theoretical Treatment of Photomixing," Applied Physics Letters, Vol. 14, No. 6 (March 1969), pp. 201-203.

7. R. J. Glauber, "The Quantum Theory of Optical Coherence," Physical Review, Vol. 130, No. 6 (June 1963), pp. 2529-2539.

8. S. C. Cohen, "Heterodyne Detection: Phase Front Alignment, Beam Spot Size, and Detector Uniformity," Applied Optics, Vol. 14, No. 8 (August 1975), pp. 1953-1959.

9. A. E. Siegman, "The Antenna Properties of Optical Heterodyne Receivers," Proceednqs of the IEEE, Vol. 54, No. 10 (October 1966), pp. 1350-1356.

10. G. Lucovsky, R. F. Schwarz, and R. B. Emmons, "Transit Time Effects in P-I-N Diodes," Journal of Applied Physics, Vol. 35, No. 3 (March 1964), pp. 622-628.

11. D. E. Sawyer and R. H. Rediker, "Narrow Base Germanium Photodiodes," Proceedings of IRE, Vol. 46, No. 6 (June 1958), pp. 1122-1130.

12. C. L. Mears, Investigation of the Quantum Efficiency of Optical Heterodyne Detectors, Ph.D. Dissertation, Dept. of Electrical Engineering, University of Virginia, Charlottesville, Va., August 1983.

13. G. Hass and L. Hadley, "Optical Properties of Metals," in American Institute of Physics Handbook, D. E. Gray, Ed., New York:McGraw-Hill Book Co., 1972, pp. 6.147-6.148.

14. R. H. Kingston, Detection of Optical and Intrared Radiation, New York: Springer-Verlag, 1979.

15. S. Ramo, J. R. Whinnery and T. Van Duzer, Fields and Waves in Communication Elctronics, New York: Wiley and Sons, Inc., 1965, pp. 294-295.

16. J. Millman and H. Taub, Pulse, Digital and Switching Waveforms, New York: McGraw-Hill Book Co., 1965, pp. 42-60.

BIBLIOGRAPHY


1. Proceedings of Heterodyne Systems and Technology, Parts I and II, NASA Publication 2138, March 25-27, 1980.

2. D. L. Spears and R. H. Kingston, "Anomalous Noise Behavior in Wide Bandwidth Photodiodes in Heterodyne and Background-Limited Operation," Appl. Phys. Lett., Vol. 34, pp. 589-590, May 1979.

3. H. R. Kowitz, "Comparative Performance of HgCdTe Photodiodes for Heterodyne Applications,"Heterodyne Systems and Technology, Part II, NASA CP-2138, 1980, pp. 297-308.

4. J. F. Shanley and C. T. Flanagan, "n-p (Hg, Cd) Te Photodiodes for 8-14 Micrometer Heterodyne Applications," Heterodyne Systems and Technology, Part II, NASA CP-2138, 1980, pp. 263-280.

5. M. B. Sirieix and H. Hofheiner, "Conceptual Design Application of HgCdTe Infrared Photodiodes for Heterodyne Systems," Heterodyne Systems and Technology PartII, NASA CP-2138, 1980, pp. 281-295.

6. C. L. Mears, "Investigation of the Quantum Efficiency of Optical Heterodyne Detectors, Ph.D dissertation, University of Virginia, Elctrical Engineering Department, Charlottesville, Virginia, August 1983.

## FIGURE CAPTIONS

Fig. 1 Two illumination schemes for p-i-n detectors.

Fig. 2 Theoretical frequency response of the drift process for silicon at $\lambda = 0.51$ μm with radiation incident from the p-side. (Non-uniform generation, two depletion widths, w = 5 μm and w = 1 μm).

Fig. 3 Theoretical frequency response of the diffusion process for silicon at $\lambda = 0.51$ μm with an impurity concentration of $4 \times 10^{16}$ cm $^{-3}$. Two depletion widths shown.

Fig. 4 Experimental optical heterodyne measurement system.

Fig. 5 Measured heterodyne efficiency for the Ford Aerospace L4502 detector using a 2.54 cm focal length focusing lens.

Fig. 6 Measured heterodyne efficiency for the detector of Fig. 5 using a 20 cm focal length focusing lens.

Fig. 7 Normalized measured efficiencies and predicted response for the detector of Fig. 4.

Fig. 8 Microwave equivalent circuit of the photodetctor and associated instrumentation.

Fig. 9 Package effects on the predicted response for the Ford Aerospace L4502. The inductor response includes effects of package inductance. The short circuit response neglects package and load effects.

Fig. 10 Predicted responses of the individual processes for the detector of Fig. 9. The depletion region response is flat over the frequencies shown.

Fig. 11 Impulse response for the Opto-Electronics PD-015-03 given by the manufacturer.

Fig. 12 Measured heterodyne efficiencies for the detector of Fig. 11 using a 2.54 cm focal length focusing lens.

Fig. 13 Measured heterodyne efficiencies for the detector of Fig. 11 using a 15.24 cm focal length lens.

Fig. 14 Normalized efficiencies for the detector of Fig. 11. The 3 dB bandwidth is approximately 1300 MHz.

Fig. 15 Impulse response for an RLC circuit with K = 0.5.

TABLE 1

L4502 SPECIFICATIONS

| | |
|---|---|
| Breakdown Voltage | 10 volts |
| Junction Capacitance | 2.5 pf |
| Series Resistance | 5 ohms |
| Light Sensitive Area | 0.01 $mm^2$ |
| Spectral Response | 0.5-1.0 um |
| Dynamic Resistance at 6 V | $5 \times 10^8$ ohms |
| Coherent Minimum Detectable Power | $<1 \times 10^{-16}$ watts |

TABLE 2

L4502 DC MEASUREMENTS

| DC EFFICIENCY | LASER | LENS FOCAL LENGTH | MEASUREMENT SET |
|---|---|---|---|
| 72 % | LEXEL | 2.54 cm | 1 |
| 51 % | COHERENT | 2.54 cm | 2 |
| 60 % | LEXEL | 2.54 cm | 2 |
| 39 % | LEXEL | 20.0 cm | 4 |
| 41 % | LEXEL | 20.0 cm | 4* |
| 37 % | COHERENT | 20.0 cm | 5 |
| 42 % | LEXEL | 20.0 cm | 5 |

* Detector realigned

TABLE 3

PD-015 SPECIFICATIONS

| | |
|---|---|
| Risetime into 50 ohms | <35 psec |
| Spectral Response | 0.3-1.1 um |
| Light Sensitive Area | 75 um x 115 um |

TABLE 4

PD-015 DC MEASUREMENTS

| DC EFFICIENCY | LASER | LENS FOCAL LENGTH | MEASUREMENT SET | OPTICAL POWER |
|---|---|---|---|---|
| 72% | COHERENT | 2.54 cm | 1 | 5 mW |
| 68% | COHERENT | 2.54 cm | 1 | 10 mW |
| 74% | COHERENT | 2.54 cm | 2 | 11 mW |
| 77% | LEXEL | 2.54 cm | 2 | 8 mW |
| 89% | LEXEL | 15.24 cm | 4 | 10 mW |
| 91% | LEXEL | 15.24 cm | 4 | 5 mW |
| 90% | COHERENT | 15.24 cm | 4 | 5 mW |
| 61% | LEXEL | 2.54 cm | 5 | 11 mW |
| 65% | LEXEL | 2.54 cm | 5 | 7 mW |
| 71% | LEXEL | 2.54 cm | 5 | 3 mW |
| 31% | COHERENT | 2.54 cm | 5 | 21 mW |
| 70% | COHERENT | 2.54 cm | 5 | 10 mW |

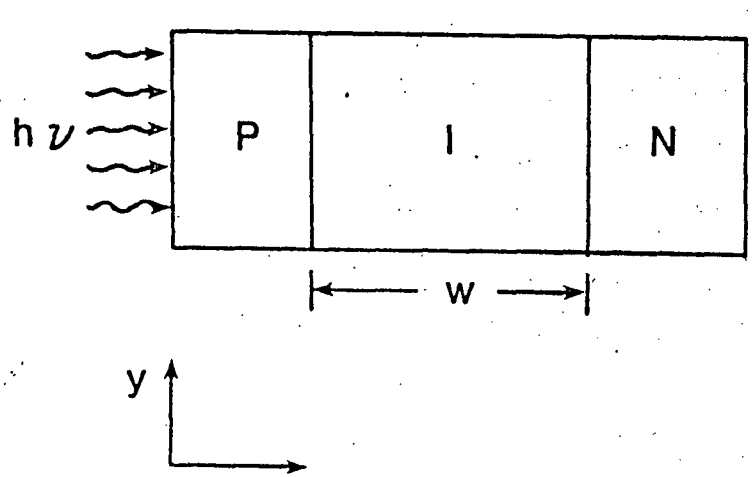


(a). Non-uniform Generation

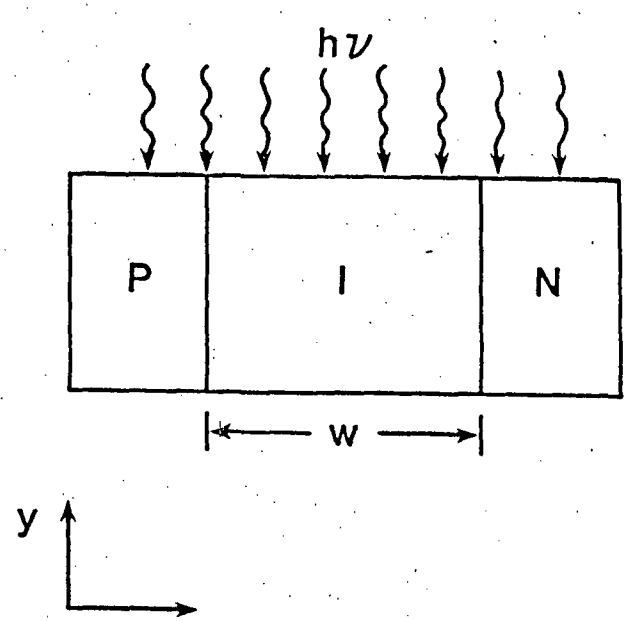


(b). Uniform Generation

ig. 1

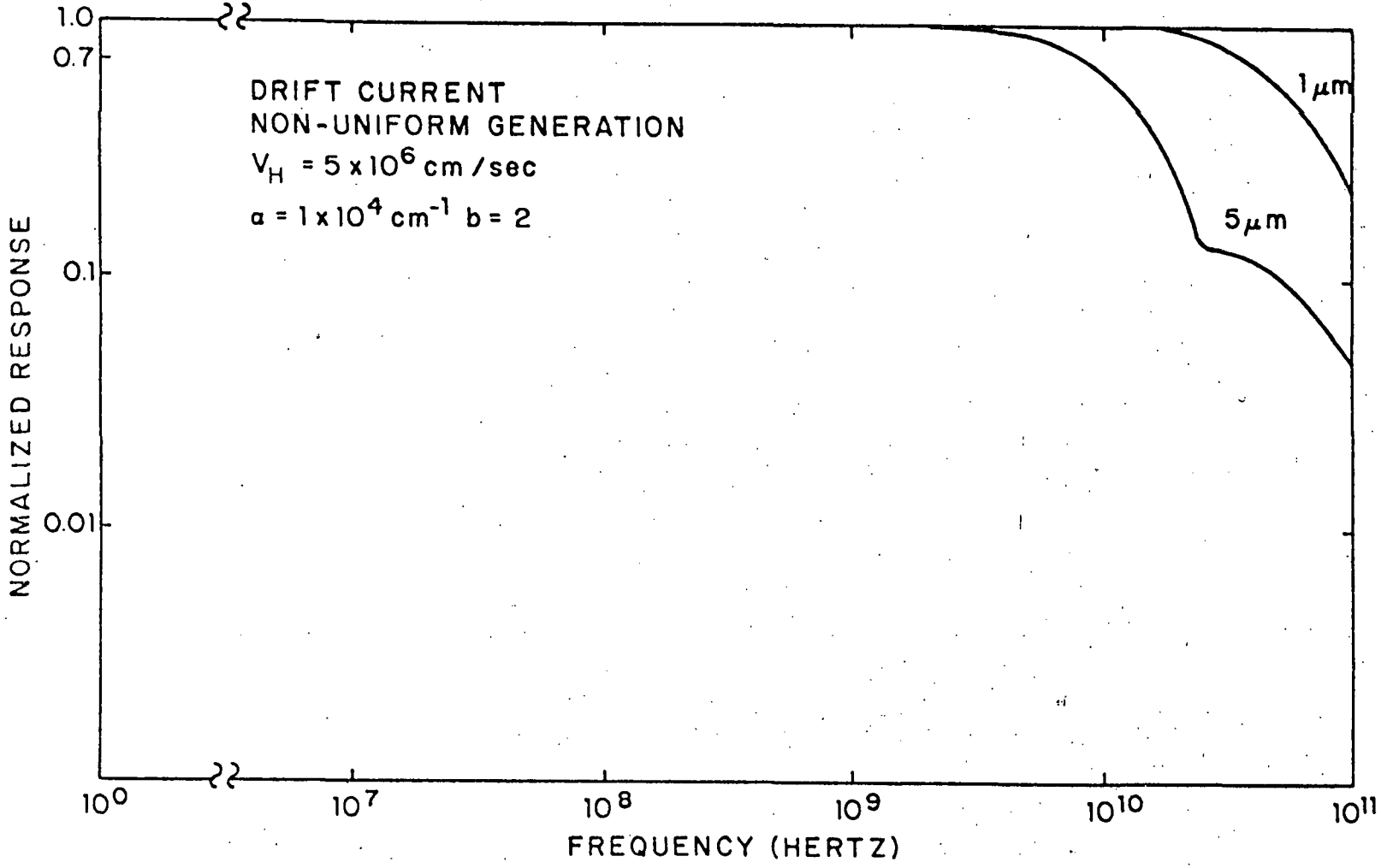
DRIFT CURRENT
NON-UNIFORM GENERATION
$V_H = 5 \times 10^6$ cm/sec
$\alpha = 1 \times 10^4$ cm$^{-1}$ b = 2
1μm
5μm
NORMALIZED RESPONSE
1.0
0.7
0.1
0.01
$10^0$
$10^7$
$10^8$
$10^9$
$10^{10}$
$10^{11}$
FREQUENCY (HERTZ)

Fig. 2

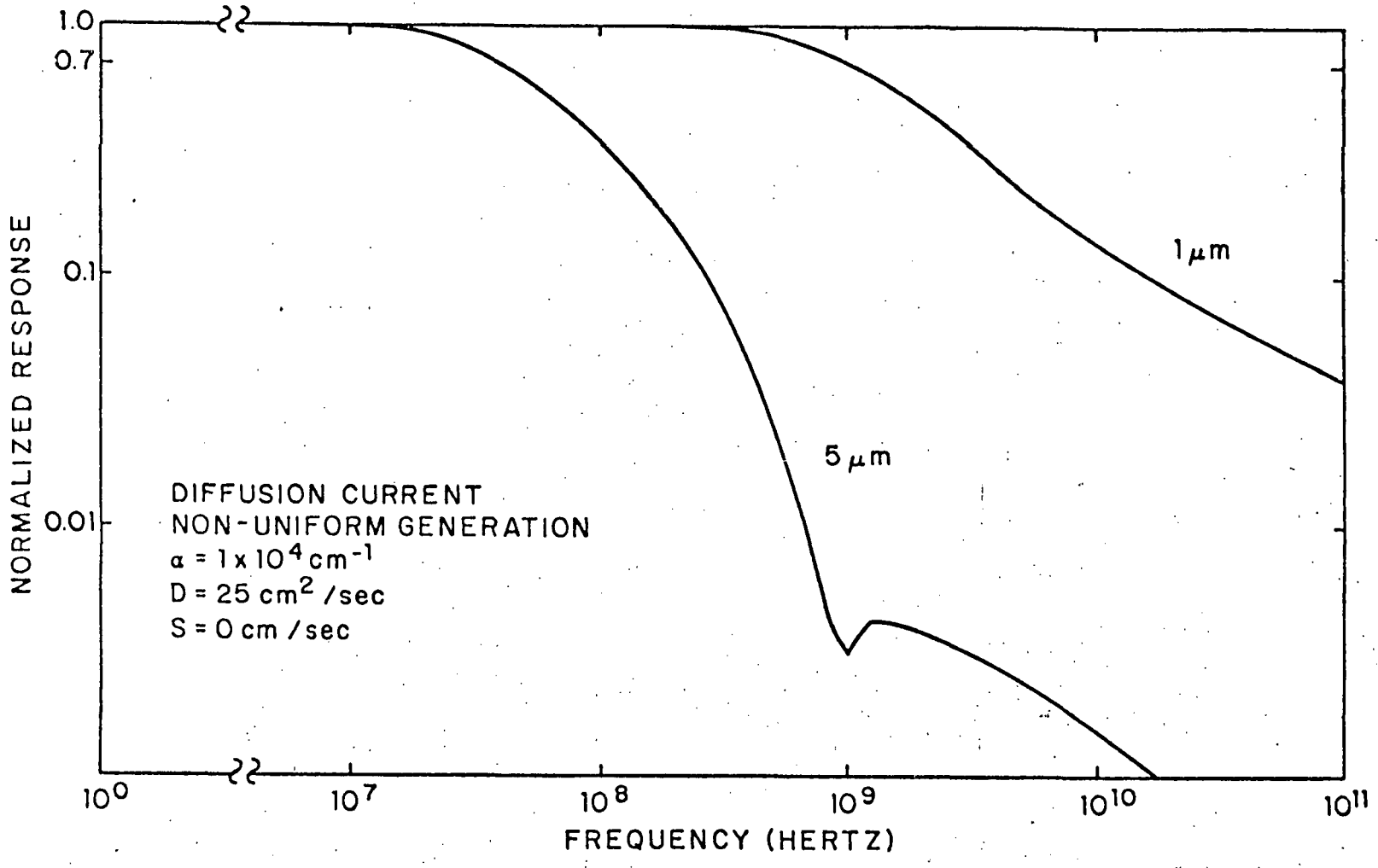
1.0
0.7
0.1
0.01
NORMALIZED RESPONSE
DIFFUSION CURRENT
NON-UNIFORM GENERATION
α = 1 x 10^4 cm^-1
D = 25 cm^2 /sec
S = 0 cm /sec
1 μm
5 μm
10^0
10^7
10^8
10^9
10^10
10^11
FREQUENCY (HERTZ)

Fig. 3

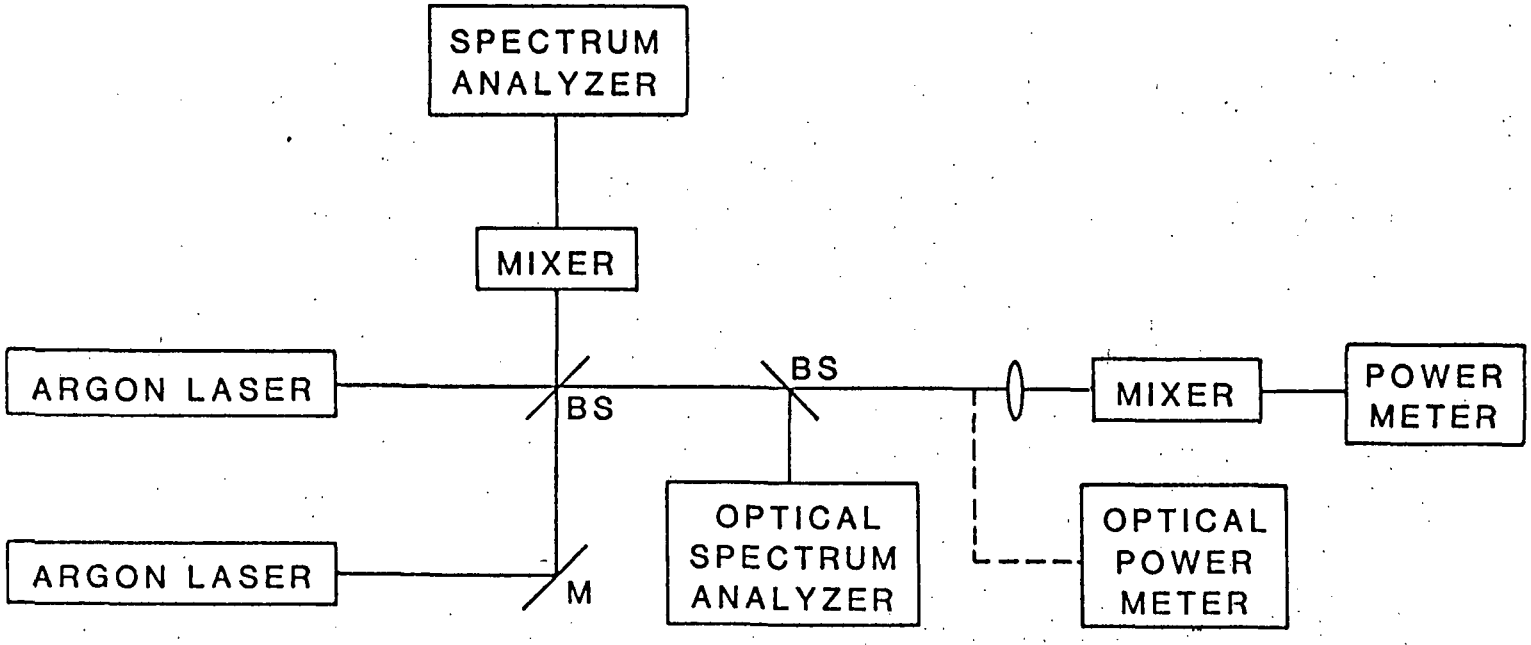
SPECTRUM ANALYZER
MIXER
ARGON LASER
BS
BS
MIXER
POWER METER
ARGON LASER
M
OPTICAL SPECTRUM ANALYZER
OPTICAL POWER METER

ig. 4

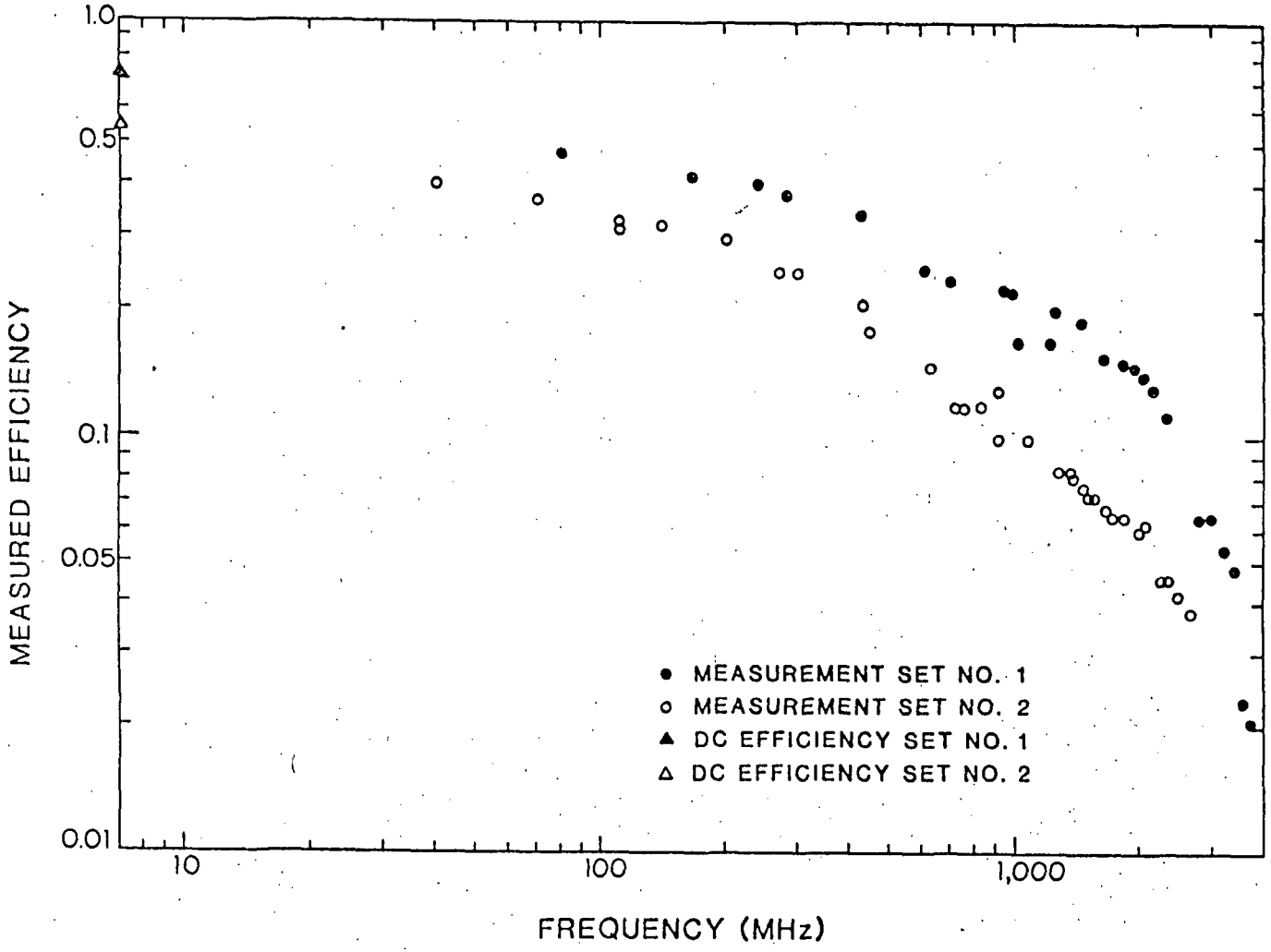
1.0
0.5
0.1
0.05
0.01
MEASURED EFFICIENCY
10
100
1,000
FREQUENCY (MHz)
MEASUREMENT SET NO. 1
MEASUREMENT SET NO. 2
DC EFFICIENCY SET NO. 1
DC EFFICIENCY SET NO. 2

ig. 5

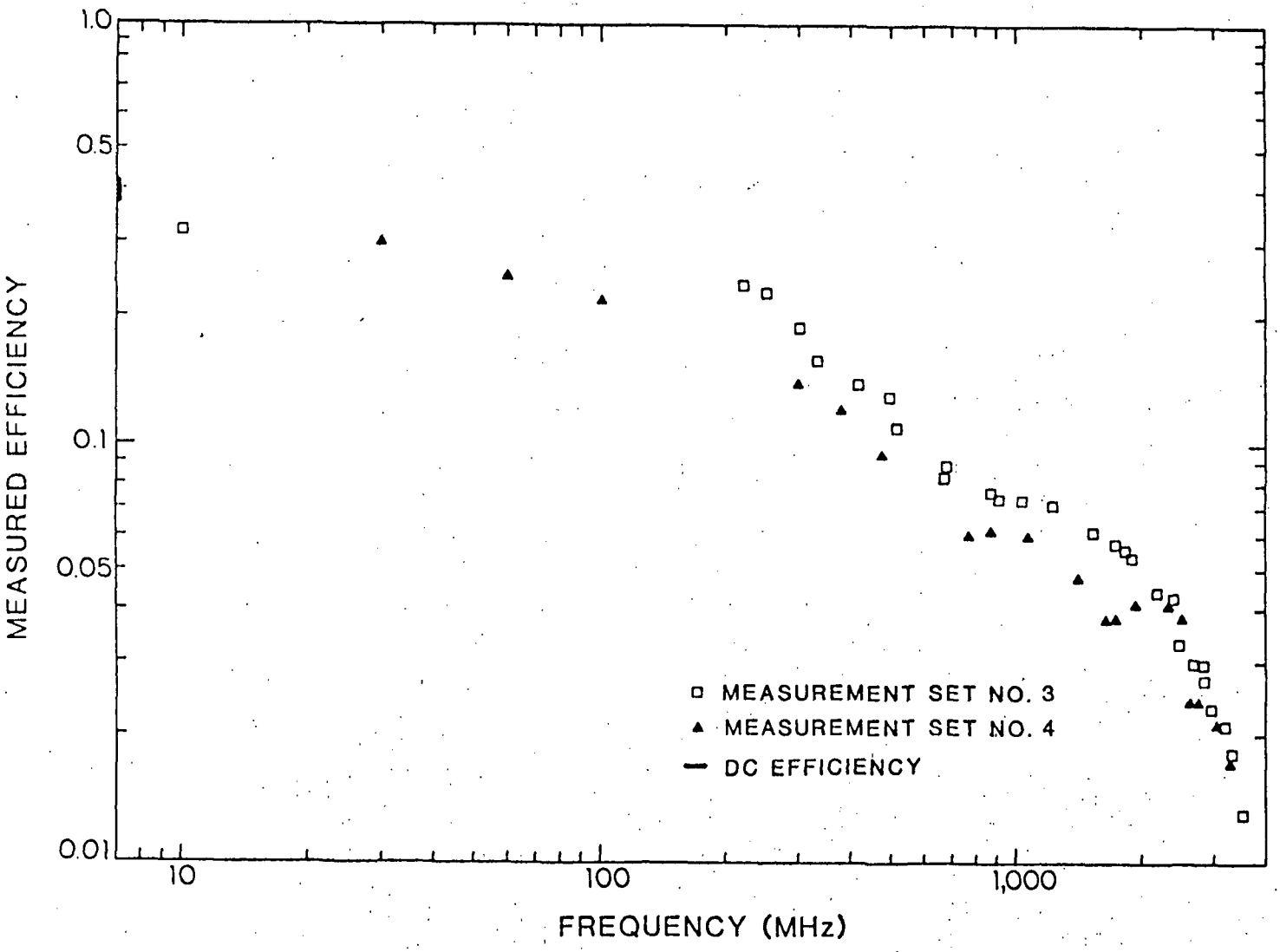
1.0
0.5
0.1
0.05
0.01
MEASURED EFFICIENCY
10
100
1,000
FREQUENCY (MHz)
MEASUREMENT SET NO. 3
MEASUREMENT SET NO. 4
DC EFFICIENCY

ig. 6

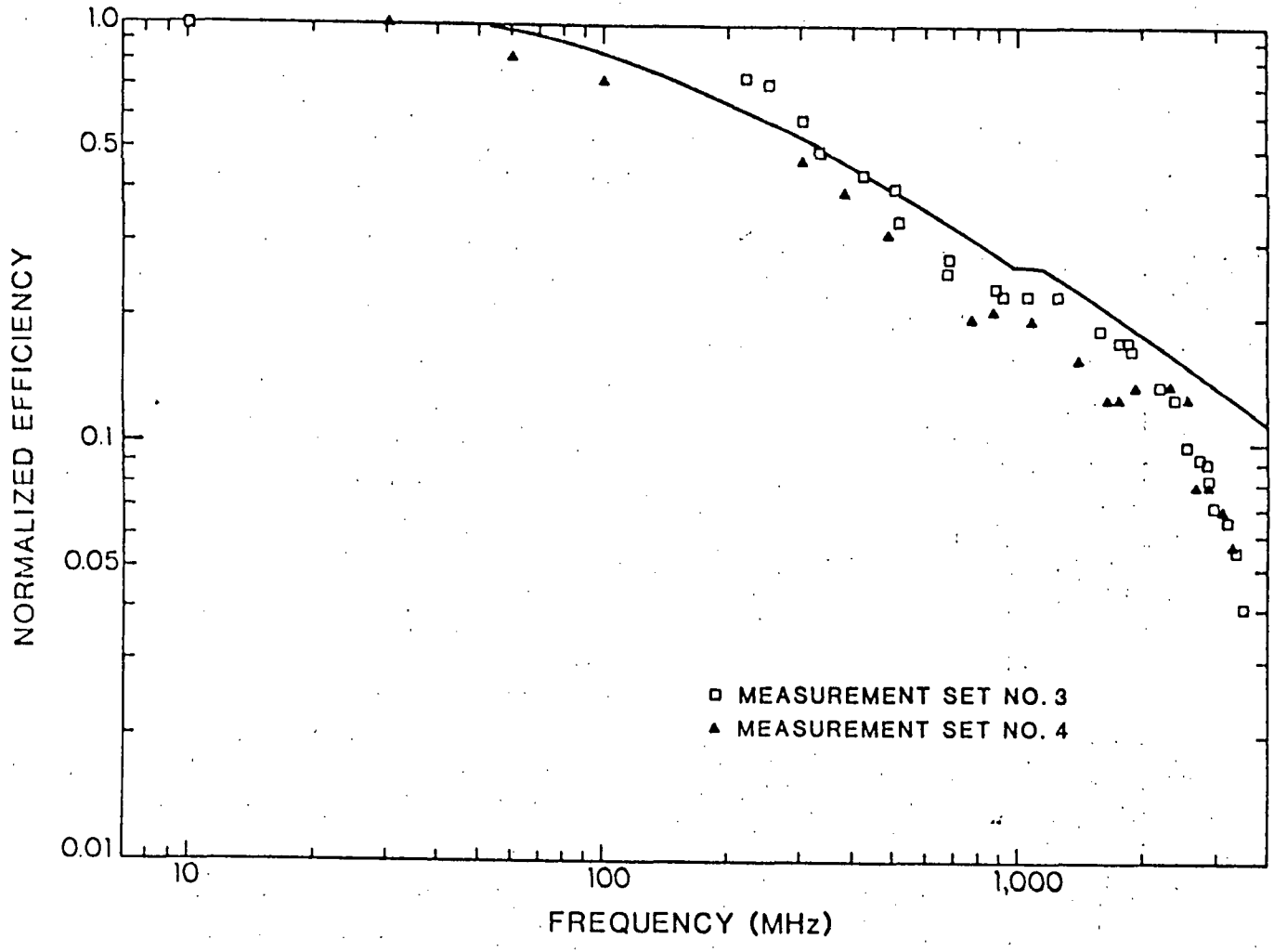
1.0
0.5
0.1
0.05
0.01
NORMALIZED EFFICIENCY
10
100
1,000
FREQUENCY (MHz)
MEASUREMENT SET NO. 3
MEASUREMENT SET NO. 4

Fig. 7

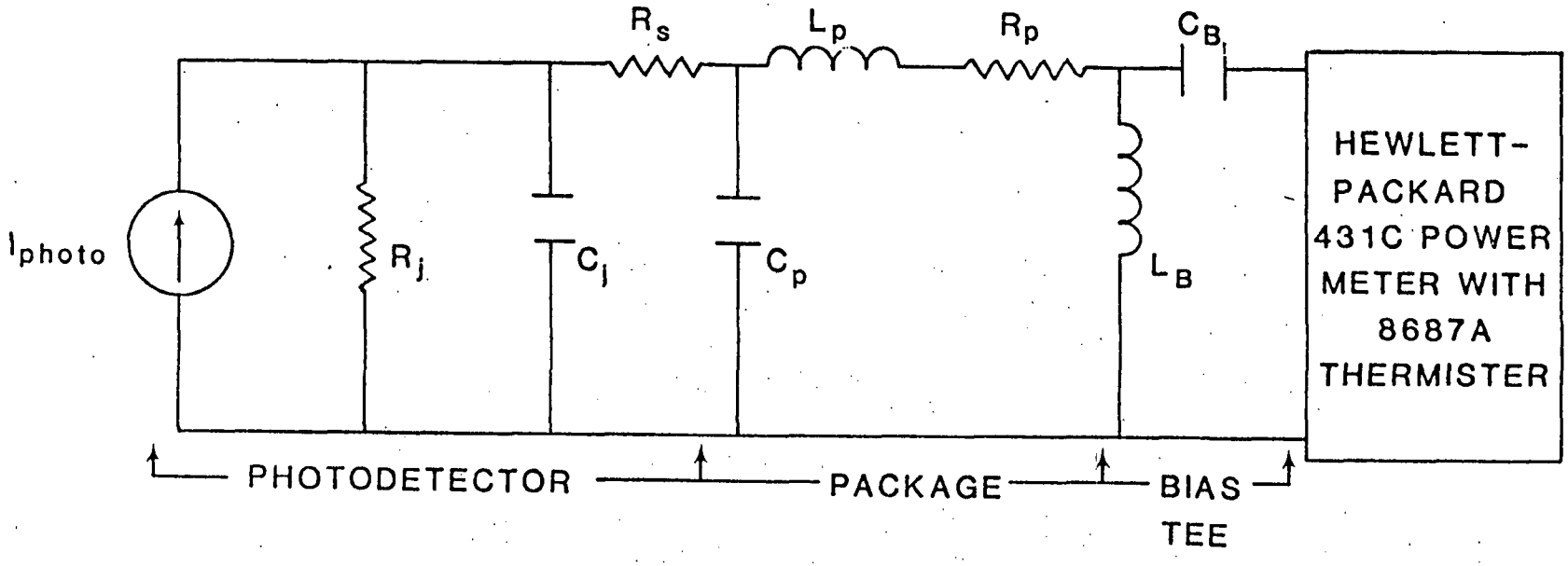
$R_s$
$L_p$
$R_p$
$C_B$
$I_{photo}$
$R_j$
$C_j$
$C_p$
$L_B$
HEWLETT-PACKARD 431C POWER METER WITH 8687A THERMISTER
PHOTODETECTOR
PACKAGE
BIAS TEE

Fig. 8

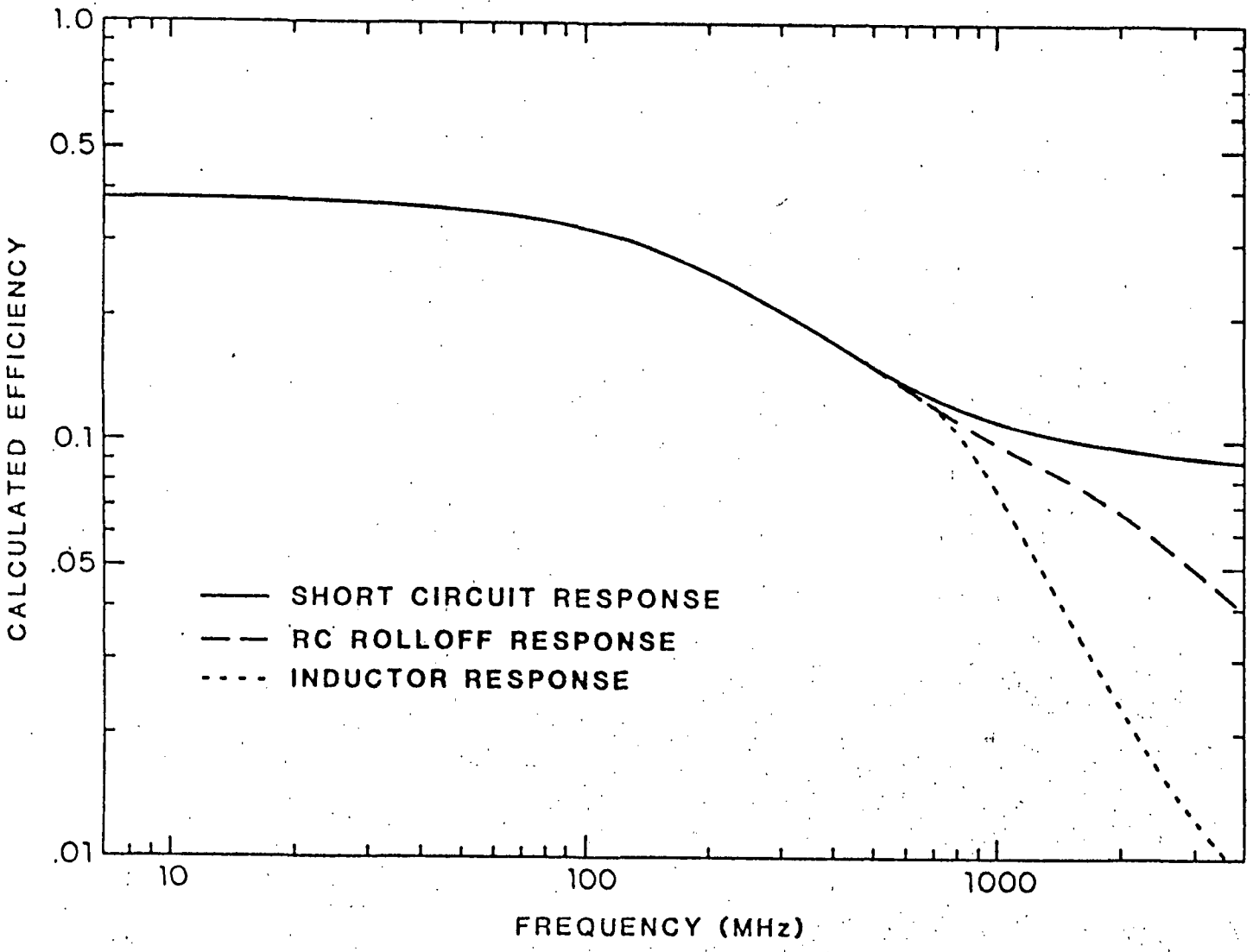
1.0
0.5
0.1
.05
.01
CALCULATED EFFICIENCY
10
100
1000
FREQUENCY (MHz)
SHORT CIRCUIT RESPONSE
RC ROLLOFF RESPONSE
INDUCTOR RESPONSE

g. 9

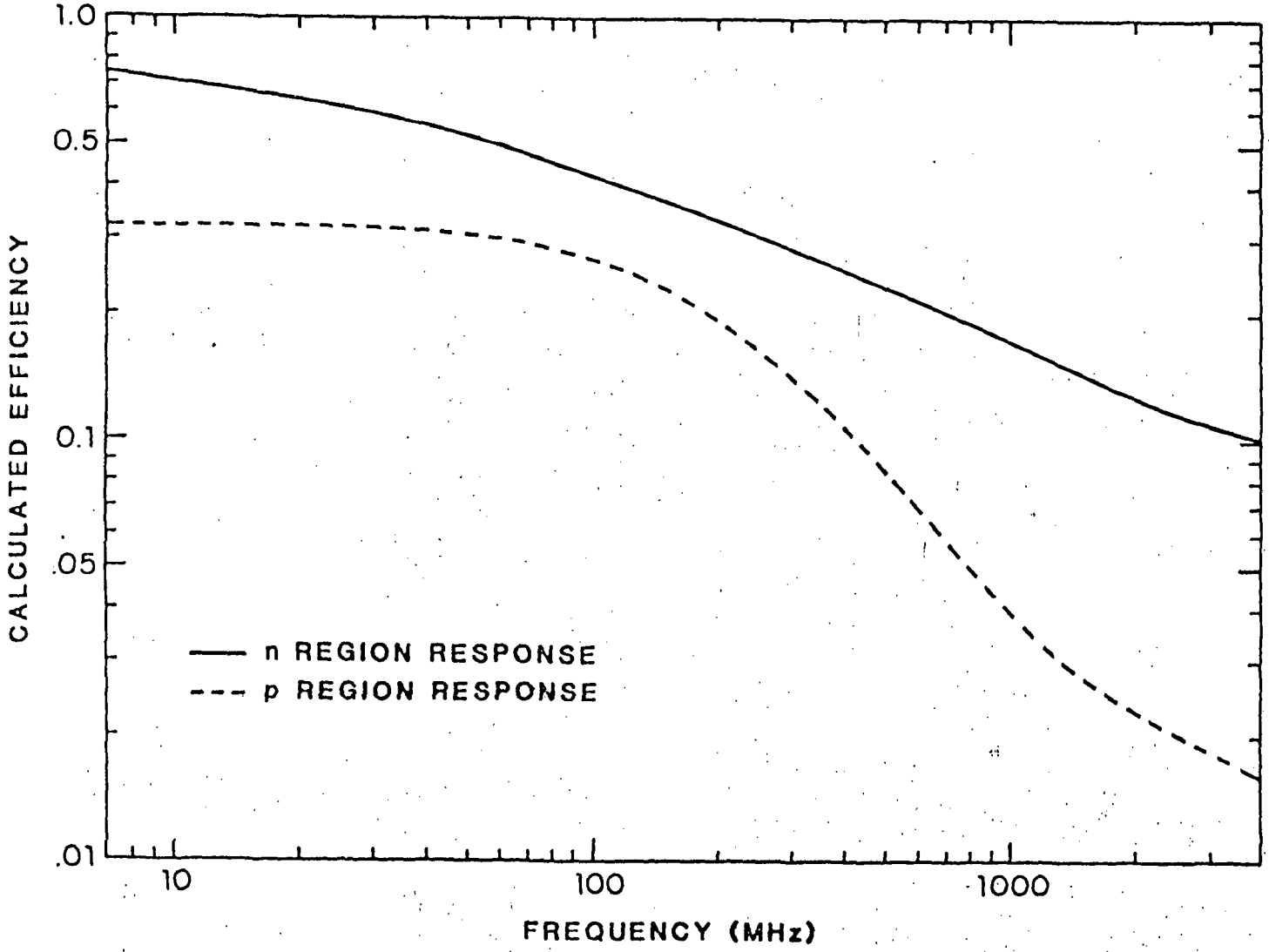
1.0
0.5
0.1
.05
.01
CALCULATED EFFICIENCY
n REGION RESPONSE
p REGION RESPONSE
10
100
1000
FREQUENCY (MHz)

Fig. 10

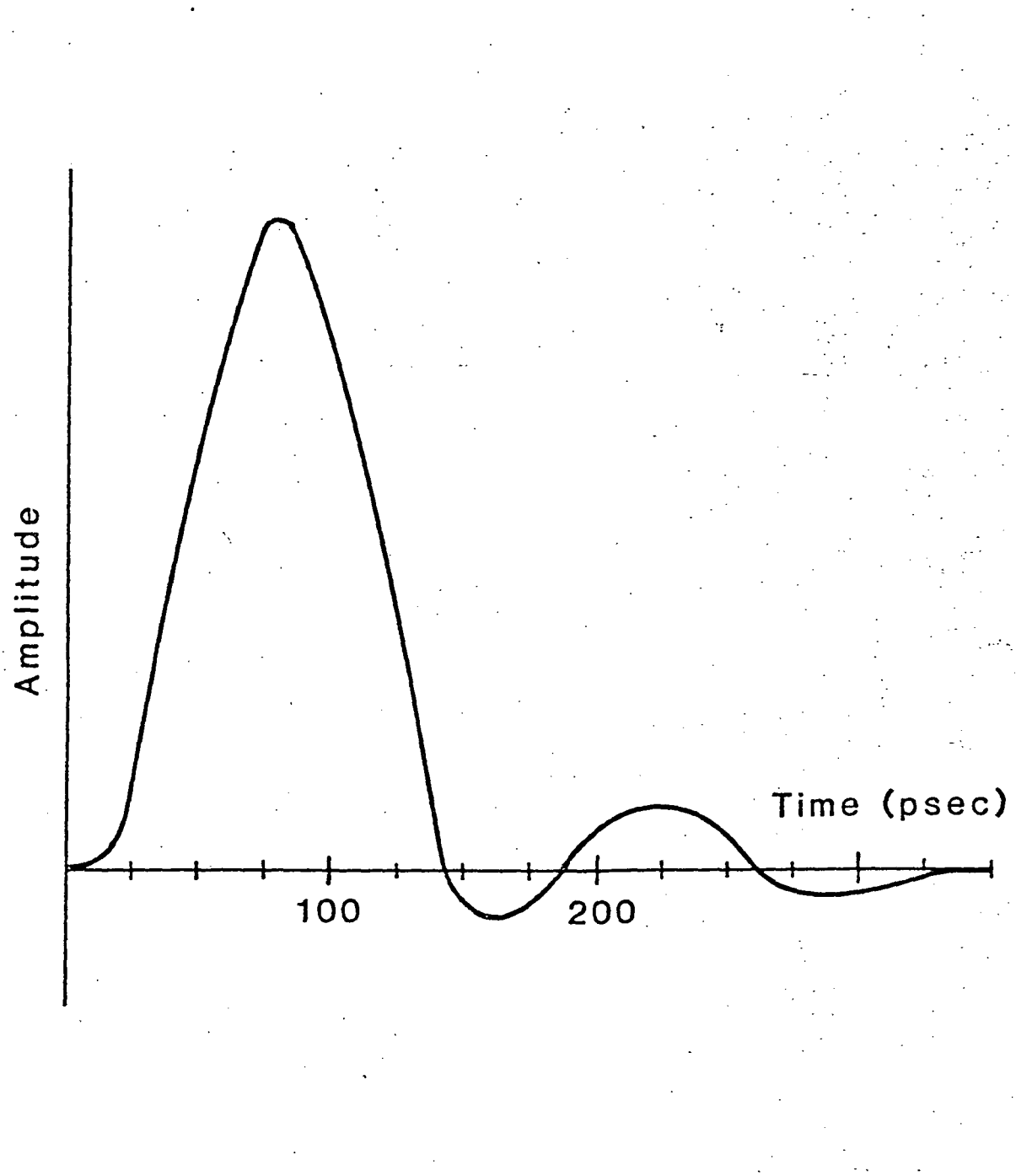
Amplitude
Time (psec)
100
200

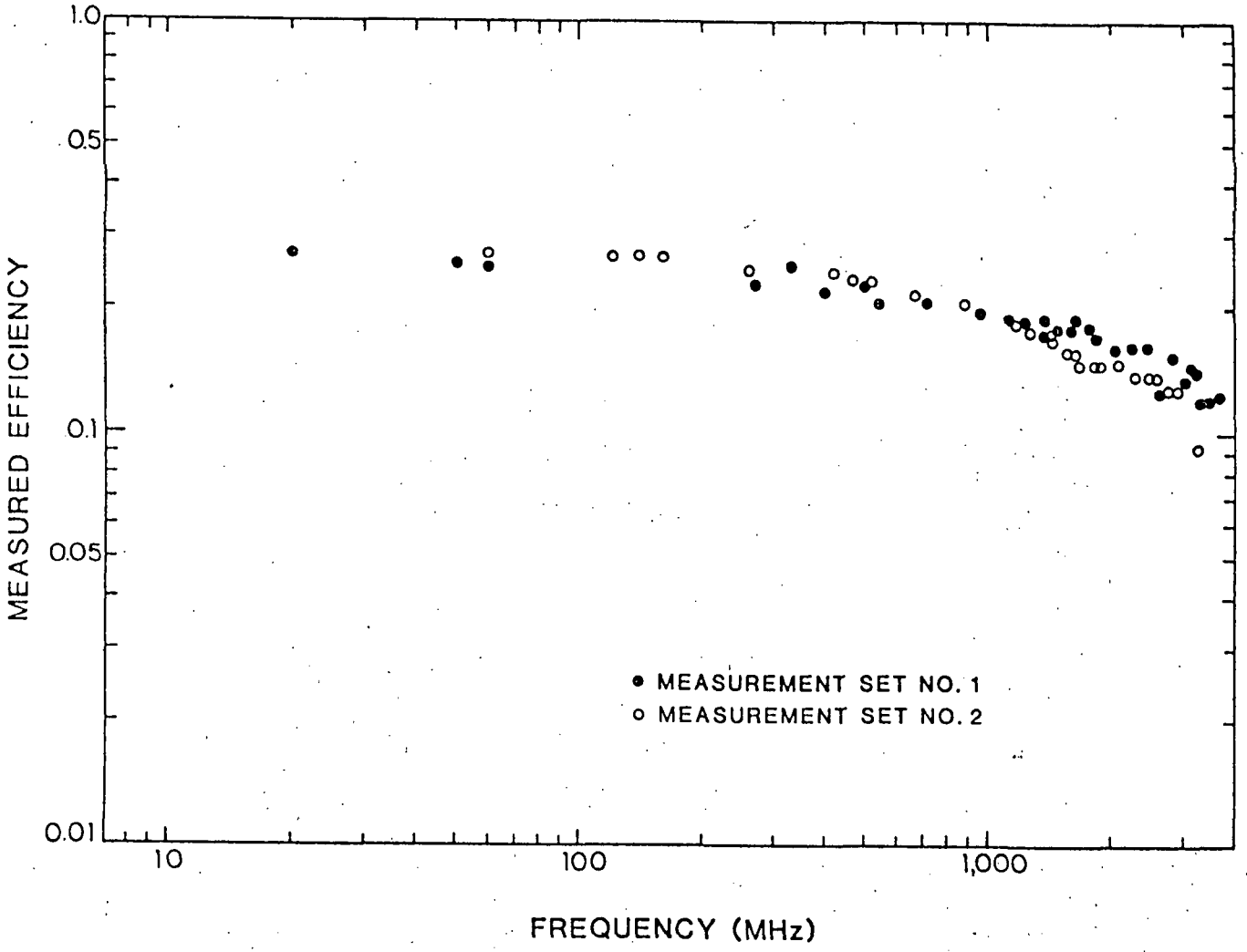
1.0
0.5
0.1
0.05
0.01
MEASURED EFFICIENCY
10
100
1,000
FREQUENCY (MHz)
• MEASUREMENT SET NO. 1
o MEASUREMENT SET NO. 2

g. 12

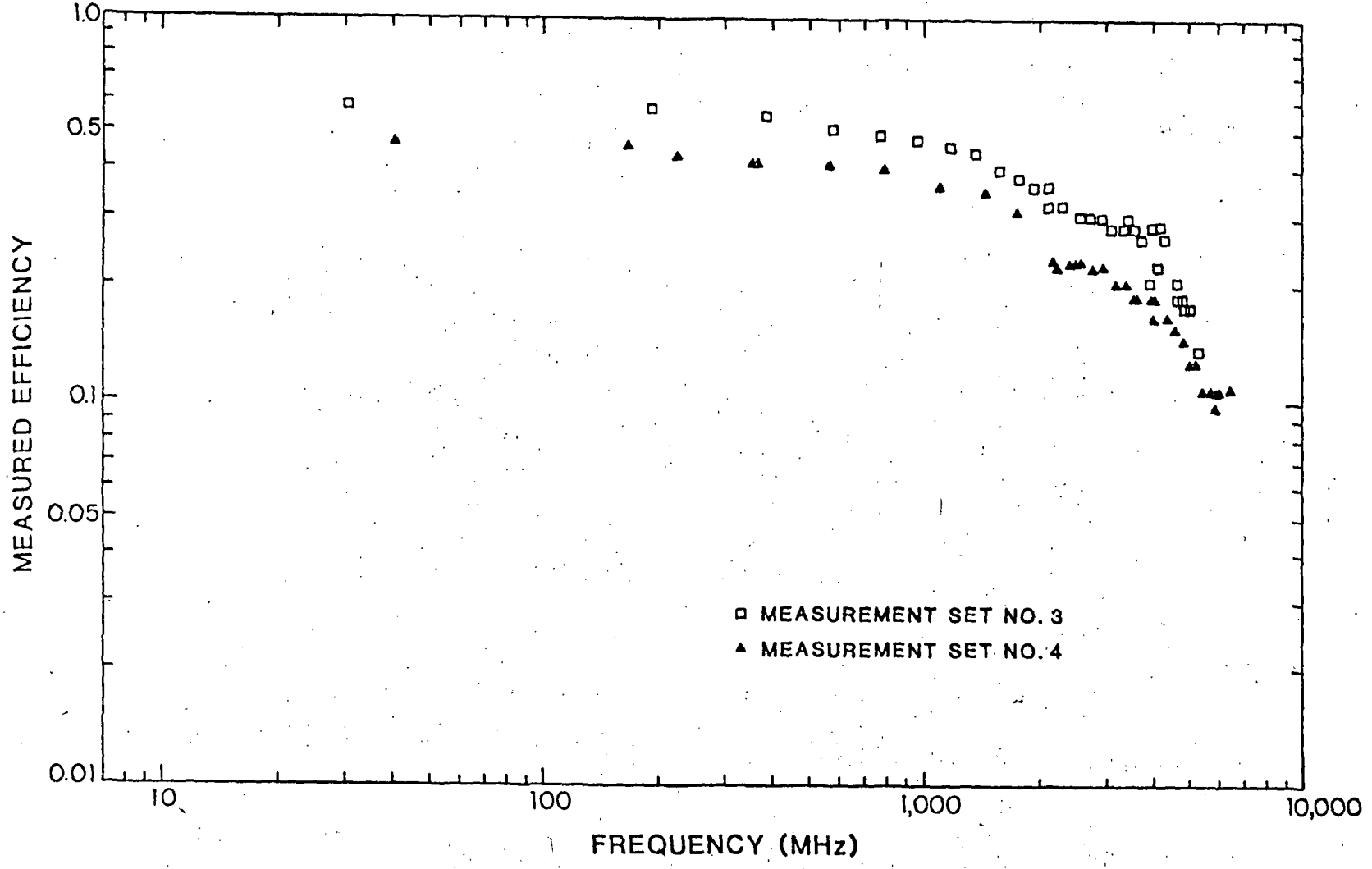
1.0
0.5
0.1
0.05
0.01
MEASURED EFFICIENCY
10
100
1,000
10,000
FREQUENCY (MHz)
MEASUREMENT SET NO. 3
MEASUREMENT SET NO. 4

Fig. 13

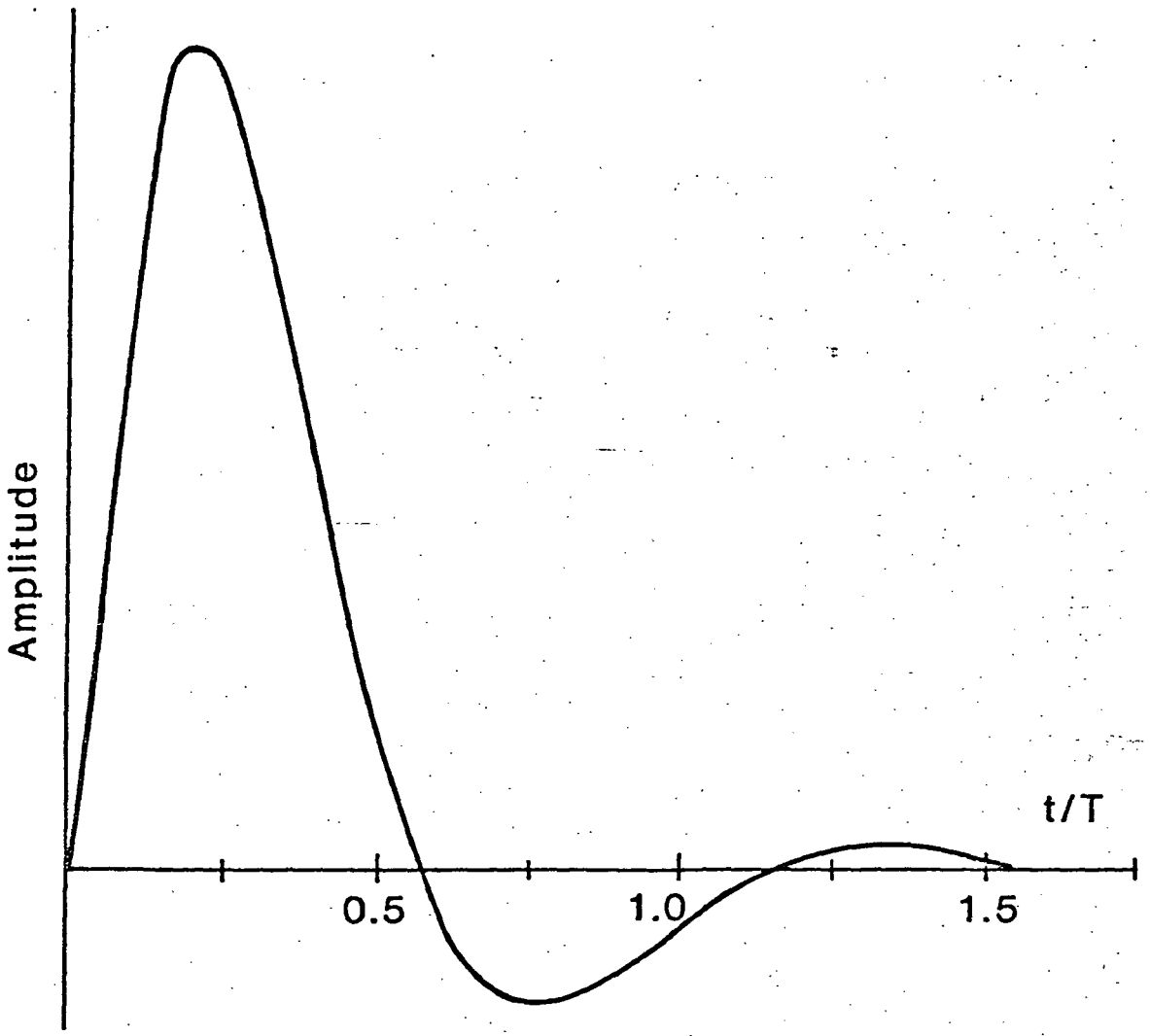
Amplitude
t/T
0.5
1.0
1.5

# DISTRIBUTION LIST

Copy No.

| | |
|---|---|
| 1 - 3 | National Aeronautics and Space Administration<br>Langley Research Center<br>Hampton, VA 23665<br><br>Attention: Mr. Daniel J. Jobson |
| 4 - 5* | NASA Scientific and Technical Information Facility<br>P. O. Box 8757<br>Baltimore/Washington International Airport<br>Baltimore, MD 21240 |
| 6 - 7 | T. E. Batchman |
| 8 - 9 | E. H. Pancake/Clark Hall |
| 10 | SEAS Files |

*One reproducible copy

5403:ccj

| 1. Report No. | 2. Government Accession No. | 3. Recipient's Catalog No. |
|---|---|---|
| | | |

| 4. Title and Subtitle | 5. Report Date |
|---|---|
| "Investigation of the Quantum Efficiency of Optical Heterodyne Detectors" | November 1984 |
| | 6. Performing Organization Code: 307-02-02-07 |
| 7. Author(s): T. E. Batchman | 8. Performing Organization Report No. |
| | 10. Work Unit No. |
| 9. Performing Organization Name and Address: University of Virginia, Charlottesville, VA | 11. Contract or Grant No.: NAG1-262 |
| | 13. Type of Report and Period Covered: Contractor Report |
| 12. Sponsoring Agency Name and Address: National Aeronautics and Space Administration, Washington, DC 20546 | 14. Sponsoring Agency Code |

15. Supplementary Notes

Langley Technical Monitor: Daniel J. Jobson

16. Abstract

This research program investigated the frequency response and quantum efficiency of optical photodetectors for heterodyne receivers. The measurements utilized two spectral lines from the output of two lasers as input to the photodetectors. These lines were easily measurable in power and frequency and hence served as known inputs. By measuring the output current of the photodetector the quantum efficiency was determined as a function of frequency separation between the two input signals. An investigation of the theoretical basis and accuracy of this type of measurement relative to similar measurements utilizing risetime was undertaken.

A theoretical study of the heterodyne process in photodetectors based on semiconductor physics was included so that higher bandwidth detectors may be designed. All measurements were made on commercially available detectors and manufacturers' specifications for normal photodetector operation are compared to the measured heterodyne characteristics.

| 17. Key Words (Suggested by Author(s)) | 18. Distribution Statement |
|---|---|
| Heterodyne, detectors | Unclassified - Unlimited<br>Subject Categories 32 & 35 |

| 19. Security Classif. (of this report) | 20. Security Classif. (of this page) | 21. No. of Pages | 22. Price |
|---|---|---|---|
| Unclassified | Unclassified | 44 | |



For sale by the National Technical Information Service, Springfield, Virginia 22161